PCCP

PAPER

View Article Online
View Journal | View Issue

Cite this: *Phys. Chem. Chem. Phys.*, 2015, **17**, 28616

Structure of P3HT crystals, thin films, and solutions by UV/Vis spectral analysis†

Marcus Böckmann,*[a] Thomas Schemme,[b] Djurre H. de Jong,[c] Cornelia Denz,[b] Andreas Heuer[c] and Nikos L. Doltsinis[a]

Received 24th June 2015,
Accepted 22nd September 2015

DOI: 10.1039/c5cp03665h

www.rsc.org/pccp

Optical absorption spectra of poly(3-hexylthiophene) (P3HT) are calculated in solution, spin-coated thin films, and the bulk crystal using a multiscale simulation approach. The structure of the amorphous thin film is obtained from coarse grained molecular dynamics (MD) simulations and subsequent back-mapping onto an atomistic force field representation. The absorption spectra are computed using TDDFT by statistically averaging over an ensemble of molecules taken from the MD simulations. Experimental UV/Vis spectra of spin-coated thin films and solutions are recorded with varying ratios of 'good' *versus* 'poor' solvent. The theoretical approach is able to faithfully predict the spectral position in the various phases and offers fundamental insight into the cause of any spectral shifts. The position of the main absorption peak is found to be chiefly determined by the level of torsion between the thiophene rings inside each molecule, while intermolecular effects are less important. Hence, optical absorption spectra hold valuable clues about the microscopic structure of disordered P3HT phases.

I. Introduction

The efficiency of bulk heterojunction solar cells critically depends on the morphology, intermolecular packing, and intramolecular conformation of the donor–acceptor mixture.[1–8] The amorphous structure of these materials is hard to characterize experimentally at an atomistic level, however indirect structural information can be gained from optical absorption and emission spectroscopy. The interpretation of photophysical properties in terms of morphology was pioneered by Kasha[9–11] and theories nowadays range from pure electronic ones to others including vibrational interaction of the monomer sites.[12,13] The latter kind was refined more recently by Silva, Spano and co-workers,[14–18] focussing on the important concept of classifying the molecular interactions into H- and J-aggregates, where J-aggregates are arranged head to tail and H-aggregates side by side. Each type gives rise to characteristic spectral signatures which can be used to extract structural information from the shape of the recorded spectrum.

Optical absorption spectra of different phases of the most often studied donor polymer for organic photovoltaics, poly(3-hexylthiophene) (P3HT, see Fig. 1 for the chemical structure), exhibit a large shift of the main absorption maximum by nearly 1 eV from the ordered crystal to the solution phase, the amorphous thin film spectrum lying inbetween.[19,20] Köhler and co-workers[21] have further shown that the spectrum of P3HT can be smoothly shifted from 'solution' to 'thin film' character in a mixture of 'good' and 'poor' solvent by increasing the amount of 'poor' (*e.g.*, ethylacetate) solvent. A dependence of the shape and position of the absorption spectrum on the chain length of the polymers has also been observed.[21,22] On the one hand, it has been suggested that the spectral changes can be understood in terms of certain types of molecular aggregates.[18,23] On the other hand, the role of the molecular conformation on spectral properties has been stressed recently.[24]

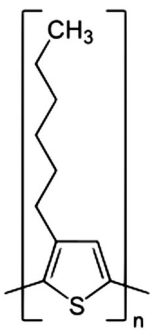

Fig. 1 Chemical structure of poly(3-hexylthiophene) (P3HT), where *n* is the number of repeat units.

[a] *Institut für Festkörpertheorie, Westfälische Wilhelms-Universität Münster and Center for Multiscale Theory & Computation, Wilhelm-Klemm-Str. 10, 48149 Münster, Germany. E-mail: marcus.boeckmann@uni-muenster.de*
[b] *Institut für Angewandte Physik, Westfälische Wilhelms-Universität Münster, Corrensstr. 2/4, 48149 Münster, Germany*
[c] *Institut für Physikalische Chemie, Westfälische Wilhelms-Universität Münster and Center for Multiscale Theory & Computation, Corrensstr. 28/30, 48149 Münster, Germany*

† Electronic supplementary information (ESI) available. See DOI: 10.1039/c5cp03665h

In this article, we present a combined theoretical and experimental study on the optical absorption spectrum of P3HT in different phases. Experimentally, UV/Vis spectroscopy has been performed on a commercially available P3HT (64.5 kDa, *i.e.* 252 repeat units) in a mixture of chloroform (good solvent) and ethylacetate (poor solvent) whose ratio is systematically varied. On the theoretical side, absorption spectra of P3HT in the ordered crystal, the amorphous solid, and in chloroform solution have been calculated using time-dependent density functional linear response theory (TDDFT)[25,26] for structures obtained from molecular dynamics simulations. Due to the long simulation times and the large system size required to generate a realistic amorphous solid phase, we first applied a coarse grained model which was then mapped back onto an atomistic representation. We demonstrate that the force field parameters have to be determined accurately from first principles calculations in order to be able to reproduce the experimental absorption spectrum. This is particularly true of the torsional potential between adjacent thiophene rings.

A detailed analysis of the effect of molecular conformation and intermolecular interaction on the absorption properties is presented. We show that the spectra hold important clues on the microscopic structure of the material. These findings will be important for the interpretation of future UV/Vis spectra and illustrate how this type of spectroscopy can provide a relatively straightforward means to characterise the structure of organic semiconductor materials.

II. Computational details

We model the P3HT polymer as an oligomer with $n = 32$ thiophene units. In the atomistic force field simulations, the CH_2 units of the hexyl side chains are treated as united atoms. In the subsequent DFT calculations, they are shortened to methyl groups.

A. Density functional theory calculations

All density functional theory calculations were performed with the Gaussian 09 Rev. D.01 quantum chemistry package.[27] Absorption spectra for the crystal were calculated using the TDDFT method with the LC-BLYP[28–30] exchange–correlation functional. For the amorphous phase and the solution, the PBE0[31] functional was used. The default basis set was 6-31G*. In each TDDFT calculation, the lowest 30 excited states were computed, covering an excitation energy range up to 4.1 eV for the crystal, 3.2 eV for the thin film, and 3.4 eV for the solution. Thus, in each case, the main absorption features are well covered by the number of states computed. For the solution, only the P3HT solute was treated explicitly, while the chloroform solvent was taken into account through a polarizable continuum model (PCM) using the integral equation formalism variant (see ref. 32 and references therein) with the united atom topological model (UAKS) as recommended for the PBE0 functional.

The solution phase absorption spectrum was calculated by averaging over ten P3HT geometries sampled every 100 ps from the second half of a 2 ns MD trajectory. For the amorphous phase spectrum, we averaged over ten single molecule spectra of randomly selected P3HT molecules from the final structure of the atomistic MD run. Environmental effects in the two solid phases were taken into account using the PCM method with relative dielectric constants of $\varepsilon = 3.0$[33] and $\varepsilon_\infty = 3.5$.[34]

B. Atomistic molecular dynamics simulations

All atomistic molecular dynamics runs were performed with the Gromacs 4.5.3 program.[35,36] *NVT* production runs were carried out at 300 K using the Gromos 45a3 force field, a timestep of 1 fs, and a Berendsen thermostat with $\tau = 0.1$ ps. For the liquid phase simulation, a P3HT 32mer was embedded in 32653 $CHCl_3$ molecules in a cubic periodic unit cell of length 15.952 nm, which is the average value from a 34 ns *NPT* equilibration run at 1 bar. Two separate Berendsen thermostats were used for the solute and the solvent, respectively. The *NVT* production run was 2 ns long.

For the amorphous bulk system, the unit cell had an average dimension of $32.16 \times 10.14 \times 10.34$ nm and contained 416 P3HT 32mers. The initial structure was obtained by back-mapping from a coarse grained simulation of a melted and refrozen crystal structure (see below). A 24 ns *NPT* run was performed using a Berendsen barostat.

The force field was partially adjusted to match DFT results. The atomic point charges were modified according to a ChelpG electrostatic potential fit[37] for the optimized tetramer with the B3LYP functional[38] and the 6-31G* basis set. In contrast to Bhatta *et al.*,[39] we distinguish head, tail, and central thiophene units as they feature different charge distributions.[40] The torsional potential between adjacent thiophene rings was reparametrized to reproduce B3LYP/6-31G* reference data for the minimum energy path along the SCCS dihedral for the dimer (see Fig. 2). The resulting low barrier for rotation is in line with other theoretical and experimental data.[40–43]

A list of all modified force field parameters is contained in Tables 1 and 2.

C. Coarse grained molecular dynamics simulations

Coarse grained molecular dynamics simulations of bulk P3HT were performed with the Gromacs version 4.6.x software.[44] The equations of motion were integrated using a leap-frog integrator with a timestep of 20 fs. Temperature was controlled using the weak coupling scheme by Bussi *et al.*[45] with $\tau_t = 1.0$ ps. The pressure was regulated to a target value of 1 bar using the weak coupling scheme by Berendsen *et al.*[46] with $\tau_p = 3.0$ ps and a compressibility of 3.0×10^{-5} bar^{-1}. Lennard-Jones (LJ) interactions were smoothly damped to zero between 0.9 and 1.2 nm. The neighbour list inside a 1.4 nm radius was updated every 10 steps.

The atomistic structure was coarse grained using a script written in-house, placing the CG beads at the center of mass of the corresponding atoms. The system was energy minmized for 100 steps using steepest descent. Subsequently the system was slowly heated to 700 K in several subsequent simulations using an anisotropic pressure coupling. At the final temperature the

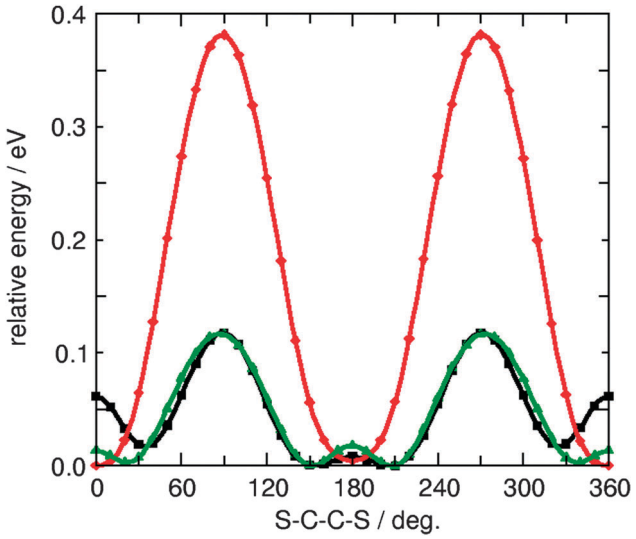

Fig. 2 Potential energy as a function of dihedral angle S–C–C–S in 2mer P3HT: *ab initio* reference (black) compared to the modified MM force field (green) and the original X–C–C–X force constant (red). The force field parameters can be found in Tables 1 and 2.

Table 1 Force field parameters used in the simulation. For the dihedral terms, the multiplicity is given in parentheses after the reference value. The S–C–C–S dihedral potential has been derived in this work (see Fig. 2), all other potentials have been taken from the Gromacs force field

Type	Reference value	Force constant	Gromacs code
C—H	1.090 Å	1.230×10^3 kJ (mol Å^4)$^{-1}$	gb_3
C–C	1.390 Å	1.080×10^3 kJ (mol Å^4)$^{-1}$	gb_15
C–S	1.780 Å	5.940×10^2 kJ (mol Å^4)$^{-1}$	gb_29
C–CH_2	1.530 Å	7.150×10^2 kJ (mol Å^4)$^{-1}$	gb_26
CH_2–CH_2	1.530 Å	7.150×10^2 kJ (mol Å^4)$^{-1}$	gb_26
CH_2–CH_3	1.530 Å	7.150×10^2 kJ (mol Å^4)$^{-1}$	gb_26
H–C–C	126.0°	575 kJ mol^{-1}	ga_35
S–C–C	126.0°	640 kJ mol^{-1}	ga_36
C–C–C	108.0°	465 kJ mol^{-1}	ga_6
C–S–C	100.0°	575 kJ mol^{-1}	ga_3
C–CH_2–CH_2	109.5°	520 kJ mol^{-1}	ga_12
CH_2–CH_2–CH_2	109.5°	520 kJ mol^{-1}	ga_12
CH_3–CH_2–CH_2	109.5°	520 kJ mol^{-1}	ga_12
S–C–C–S	180.0° (2)	2.50 kJ mol^{-1}	This work
X–C–C–X	180.0° (2)	5.86 kJ mol^{-1}	gd_1
X–C–S–X	180.0° (2)	5.86 kJ mol^{-1}	gd_1
C–C–CH_2–CH_2	0.0° (6)	3.77 kJ mol^{-1}	gd_21
C–CH_2–CH_2–CH_2	0.0° (3)	5.86 kJ mol^{-1}	gd_17
CH_2–CH_2–CH_2–CH_2	0.0° (3)	5.86 kJ mol^{-1}	gd_17
CH_3–CH_2–CH_2–CH_2	0.0° (3)	5.86 kJ mol^{-1}	gd_17

pressure coupling was set to isotropic and the system simulated for 200 ns.

Subsequently, the molten system was cooled back to 500 K using simulated annealing at a rate of 0.2 deg ns^{-1} with anisotropic pressure coupling. The final structure was back-mapped to the united-atom level using the backmapping procedure as described in ref. 47.

The coarse grain topologies were based on the Martini force field.[48] Initial parameters were obtained from ref. 49.

Table 2 Force field charges used in the simulations. The charges were first calculated from DFT and subsequently rounded so that the charges within a charge group add up to zero. Side chain atoms have zero charge in the united atom model

Type	Head	Body	Tail
S1	0.00	−0.15	0.00
C2	−0.10	0.00	−0.10
C3	0.20	0.10	0.10
C4	−0.20	0.20	0.20
C5	−0.10	0.15	0.00
H(C2)	n/a	n/a	0.10
H(C4)	0.10	0.10	0.10
H(C5)	0.10	n/a	n/a

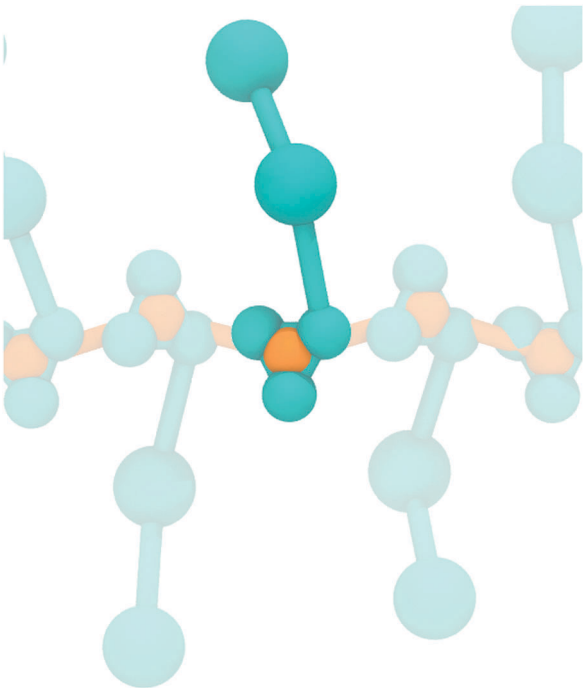

Fig. 3 Snapshot of a coarse grain representation of the P3HT polymer. The monomer (highlighted) consist of five beads (cyan) and one virtual site (orange).

The molecule is described by three particles and one virtual site for the thiophene ring, for numerical stability, and two particles for the hexyl chain (Fig. 3). The virtual site has no LJ interaction with other beads and is positioned at the center of mass of the three ring particles. In order to correctly reproduce the density and stacking of the crystal,[50] the LJ σ for the self-interaction was reduced from 0.47 to 0.42 nm for the tail particles and to 0.32 nm for the ring particles (S- and T-type particles in the Martini force field, respectively).

III. Experimental details

All experimental investigations are based on a commercially available P3HT (Plexcore OS 2100) with an average molecular weight of M_n = 64.5 ± 10.5 kDa. For the determination of thin film absorbance of layers of P3HT, solutions of P3HT in

chloroform at a concentration of 10 mg ml^{-1} were prepared. Thin films were fabricated by means of spin coating of the solutions onto microscope slides. The spinning speed was adjusted to 10 rps. Spectra of the films were taken by a Jasco V-530 UV/Vis spectrometer with an additional mask in the beam path to seize the illuminated area of each sample.

For the preparation of solutions with different ratios of good and poor solvent, a stock solution of P3HT in chloroform at 10 mg ml^{-1} was prepared. To enhance the solubility, the stock solution was annealed slightly (by *ca.* 25 degrees) above room temperature for five minutes. After complete dissolution of the material, the concentration was adjusted to 1 mg ml^{-1} and further diluted by subsequently adding chloroform and ethylacetate to get the final concentration of 10 mg mol^{-1} at the desired solvent ratios. Several different ratios of chloroform and ethylacetate were realized. Contents of ethylacetate of more than 25% resulted in strong precipitation of the polymer and the formation of large aggregates resulting in reduced overall absorbance due to the strong dispersive and sedimentative behavior. For characterization, the different solutions were filled in fused silica cuvettes of 1 mm thickness and the spectra were taken by a Jasco V-530 UV/Vis spectrometer.

IV. Results and discussion

A. Experimental absorption spectra in mixed solvent

Fig. 4 presents the UV/Vis spectrum of a commercial P3HT (see Section III) dissolved in chloroform together with data obtained for solutions with increasing content of ethylacetate. It is seen that — up to a content of 7% of the 'poor' solvent — the spectrum shows the typical featureless absorption band of dissolved P3HT with a maximum at about 2.8 eV. The spectrum remains largely unchanged when the measurement is repeated after 24 hours, see dashed line in Fig. 4. Starting with a content of 10% ethylacetate, the spectrum is significantly red-shifted and displays the features of the 'thin film' spectrum with distinguished features at 2.0, 2.2, and 2.4 eV, the contribution from the 'ideal solution' being extinguished at 25% ethylacetate. Further increase of ethylacetate content yields a strong aggregation with 'phase separation' putting the sample in an optically very dense state. These findings are in line with results reported for medium-sized P3HT oligomers in a similar solvent mixture series[21] and are attributed to the formation of polymer chain aggregates and resulting inter-chain interactions. Similar aggregate formation has been observed for P3HT suspensions in tetrahydrofuran/water[51] and in temperature-dependent experiments of P3HT in isodurene[16] (see also Table S1 in the ESI†).

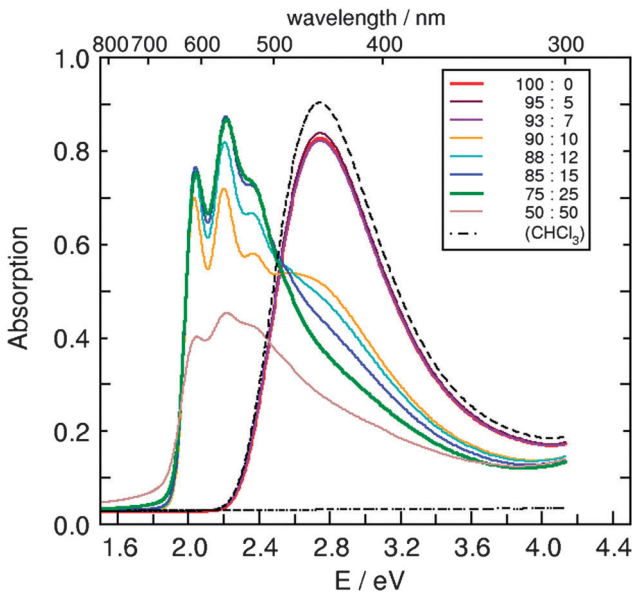

Fig. 4 UV/Vis spectra of P3HT in $CHCl_3$/ethylacetate solvent mixtures of varying ratio. The dashed line represents the 100 : 0 mixture after 24 h.

B. Theoretical absorption spectra

1. Ordered crystal. Fig. 5a shows the theoretical UV/Vis spectrum of 32meric P3HT in the crystal geometry published in ref. 50. It is seen to agree fairly well with the experimental data by Rahimi *et al.*[20] The crystal spectrum was first calculated with TDDFT using the LC-BLYP functional and the 6-31G* basis set for a single, planar, regioregular oligomer. A shift of −0.04 eV to account for basis set incompleteness was then determined by recalculating the lowest energy absorption peak with the 6-31+G* basis set for the 5mer, 10mer, and 20mer and extrapolating to the 32mer. A test calculation on the 5mer with the cc-pVTZ basis set yielded an only marginally lower excitation energy (by 0.02 eV) than 6-31+G*. Due to the extent of electron delocalization in this planar configuration (see Fig. 6), use of a

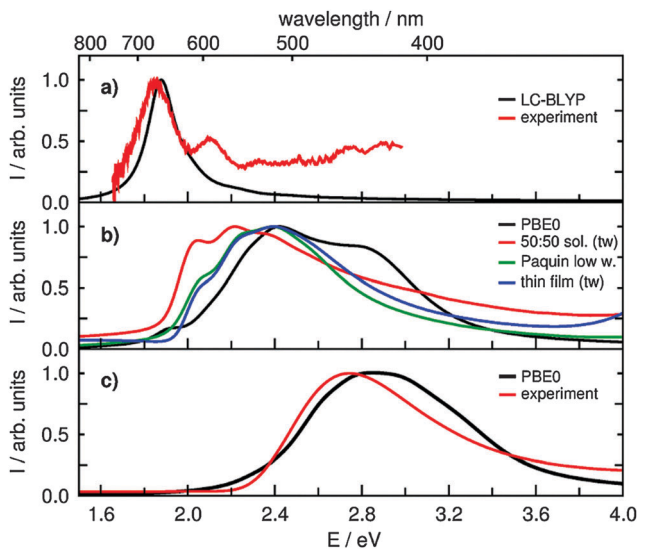

Fig. 5 Comparison of experimental and theoretical absorption spectra of P3HT in an ordered crystal (a), an amorphous phase (b), and in solution (c). The intensity *I* has been normalized and is given in arbitrary units. The experimental spectrum in (a) was measured by Rahimi *et al.*[20] Panel (b) contains experimental data from this work for a solution with 50% good solvent and 50% poor solvent (red line) and a spin coated thin film (blue line); the green line is the low molecular weight thin film data by Paquin *et al.*[22] The experimental data in (c) has been recorded in this work for a solution with 100% good solvent.

long-range corrected functional is essential to obtain accurate excitation energies. In the present case, the LC-BLYP functional produced slightly better agreement with experiment than, for instance, CAM-B3LYP (see ESI,† Fig. S1).

It is well known that the spectral position depends crucially on the length of the P3HT oligomer. The Kuhn extrapolation formula for excitation energies,[52]

$$E = E_0\sqrt{1 + 2\frac{\kappa'}{\kappa_0}\cos\left(\frac{\pi}{2n+1}\right)} \quad (1)$$

where n is the number of thiophene units in the chain, E_0, κ_0, and κ' are the vibrational energy, force constant, and coupling constant of the C=C double bonds, respectively, is commonly used to describe the dependence of the excitation energy on the chain length. However, according to eqn (1), the excitation energy for the chain length used in the present calculations (n = 32) is already close to the asymptote for large n. In fact, the excitation energy for n = 250 is only 0.02 eV lower than that for n = 32.

The overall spectral shape can be understood in terms of one-electron excitations between the molecular orbitals of the

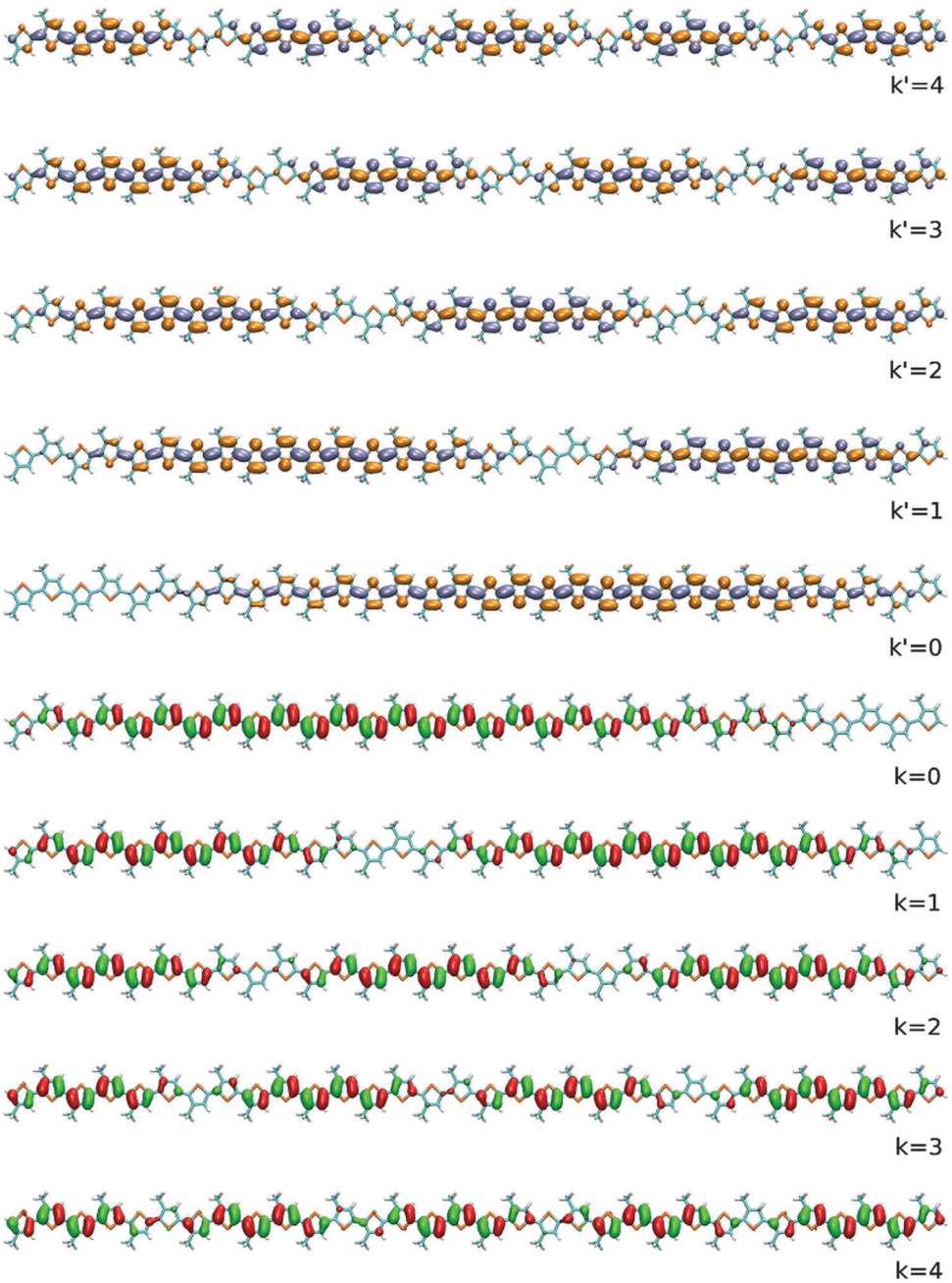

Fig. 6 Frontier molecular orbitals (MOs) of planar 32mer P3HT calculated with LC-BLYP/6-31G* from LUMO+4 (k' = 4) to HOMO−4 (k = 4) (top to bottom) showing s-type (virtual MOs) and p-type (occupied MOs) band character, respectively.

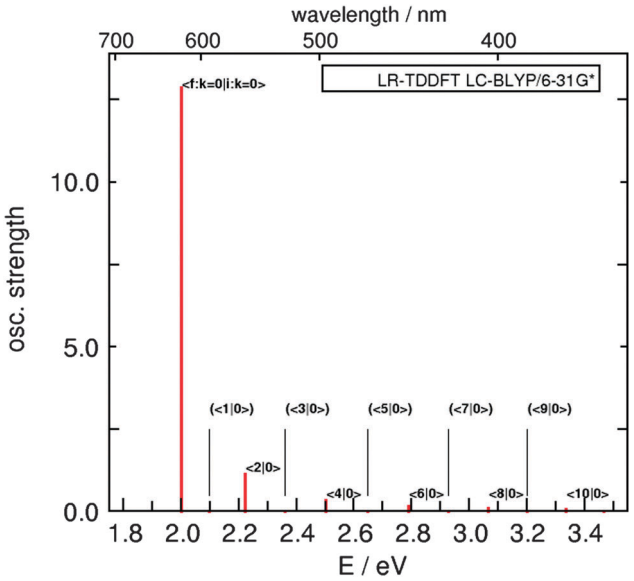

Fig. 7 Planar 32-mer P3HT:TDDFT/LC-BLYP/6-31G* line spectrum; labels indicate the leading contribution to the transition moment. Note that transitions ⟨odd|0⟩ vanish due to symmetry considerations.

polymer depicted in Fig. 6. As illustrated in Fig. 7, the main peak (here at ≈2.0 eV) originates from a HOMO–LUMO excitation, *i.e.* $k = 0 \rightarrow k' = 0$ following the notation introduced in Fig. 6. Since both HOMO and LUMO are considerably delocalized, it is clear that the spectrum is red-shifted compared to that of a single thiophene unit. It should be noted that the frontier orbitals of the polymer can be thought of as linear combinations of the monomer HOMO and LUMO, respectively. Visualizations of the monomer frontier orbitals can be found in Fig. S9 of the ESI.†

The second peak, with much lower intensity (here at ≈2.2 eV), can be assigned to a $k = 0 \rightarrow k' = 2$ transition, while the third peak at about 2.5 eV, with lower intensity still, arises from a $k = 0 \rightarrow k' = 4$ transition. In summary, the series of $S_0 \rightarrow S_{2n}$ ($n = 1, 2, \ldots$) excitations can be described as $k = 0 \rightarrow k' = 2n$ transitions whose oscillator strength decays exponentially with n.

Furthermore, it is apparent from Fig. 7 that transitions between $k = 0$ and odd k' values have near zero intensities. Looking at the shape of the molecular orbitals (Fig. 6), it becomes clear that such transitions are symmetry-forbidden due to the fact that orbitals with odd k' have an odd number (namely k') of 'super-nodes', while the HOMO ($k = 0$) has no 'super-nodes'.

Although we have seen good agreement between the theoretical spectrum in the single molecule approximation and the experimental signal (see Fig. 5a), the question remains how the crystal environment affects the molecular absorption. For this reason, we have performed an analogous calculation on a dimer of two neighbouring 32mers cut out from the crystal. The main peak of the dimer was found to be red-shifted by less than 0.01 eV relative to the single molecule. The validity of the single molecule approximation is further confirmed by comparing the spectra obtained with and without taking into account the crystal environment using the PCM method. The spectra are seen to be very similar, the PCM only producing a minor red-shift of about 0.03 eV (see ESI,† Fig. S2). This is in line with the expectations from theoretical models[53] which predict the interchain effect to vanish with increasing chain length.

2. Amorphous solid. An amorphous solid bulk structure of P3HT was generated in a multiscale fashion by combining coarse grained and atomistic MD simulations and quantum-chemical TDDFT calculations as described in Section II. Fig. 5b shows the ensemble-averaged optical absorption spectrum of the amorphous phase at 300 K obtained with TDDFT/PBE0/6-31G* in the single molecule approximation. The theoretical spectrum is in fair agreement with the experimental spectrum recorded by Paquin *et al.*[22] for thin films of P3HT oligomers with low molecular weight (12.4 kDa, *i.e.* $n = 48$) and our experimental spectrum for a higher molecular weight of 64.5 kDa. There is no red-shift with increasing molecular weight as observed by Paquin *et al.*[22] as the two experimental thin film spectra virtually lie on top of each other. Since this effect was seen between molecular weights of 12.4 and 264 kDa, the P3HT chains used in the present work may be too short (64.5 ± 10.5 kDa) for the shift to occur. The slight overall blue-shift of the theoretical spectrum relative to the experimental thin film spectra can be partially explained by the fact that the hexyl groups were replaced by methyl groups in the calculations and a smaller basis set (6-31G*) was used. For the crystal structure, we determined a blue-shift of 0.1 eV due to these effects. It is remarkable, however, that the main absorption maximum of the theoretical curve coincides with those of the two experimental thin film spectra. The shoulder in the theoretical spectrum at about 2.8 eV is less pronounced and the maximum is slightly blue-shifted when the calculations are performed in vacuum, *i.e.* without the PCM method (see ESI,† Fig. S3).

The spectrum labelled 50 : 50, which is also included in Fig. 4, representing the precipitated P3HT in an equal mixture of 'good' and 'poor' solvent, on the other hand, appears slightly red-shifted and more structured (Fig. 5b), exhibiting three distinct features around 2.0, 2.2, and 2.4 eV. One could argue that the overall red-shift of the band results from a reweighting of the intensities of the three sub-peaks. The characteristic shape of this band with its distinguished features has been observed for P3HT of various chain lengths, different degrees of regio-regularity,[54] as well as for P3HT nanofibers.[55] (See Table S1 of the ESI† for a survey of literature data.)

Interestingly, the shoulder around 2.0 eV, which has been assigned to a 0–0 transition of an H-aggregate of regio-regular P3HT in the literature (see, for example, ref. 18), is also found in thin films of regio-random P3HT.[56] The dominant higher energy part of the spectrum is usually thought to arise from more disordered chains.[18]

Compared with the ordered crystal (Fig. 5a), the spectrum of the amorphous solid is blue-shifted and broadened. Analysis of the molecular conformations obtained from our molecular dynamics simulations reveals a considerable degree of torsion between neighbouring thiophene rings, which is owed to the rather flat potential along this coordinate (see Fig. 2).

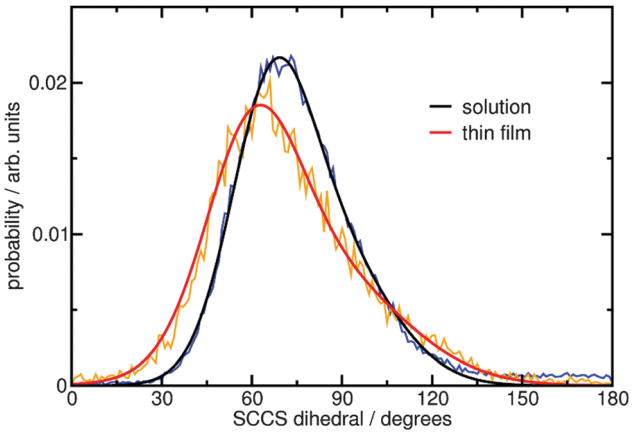

Fig. 8 Distributions of absolute SCCS dihedral angles, θ, relative to the ideal planar regioregular geometry. The histogram data for the thin film and the solution (orange and blue lines, respectively) is shown together with Gaussian fits of the form $a_1e^{-(\theta-b_1)^2/c_1} + a_2e^{-(\theta-b_2)^2/c_2}$ (red and black lines, respectively).

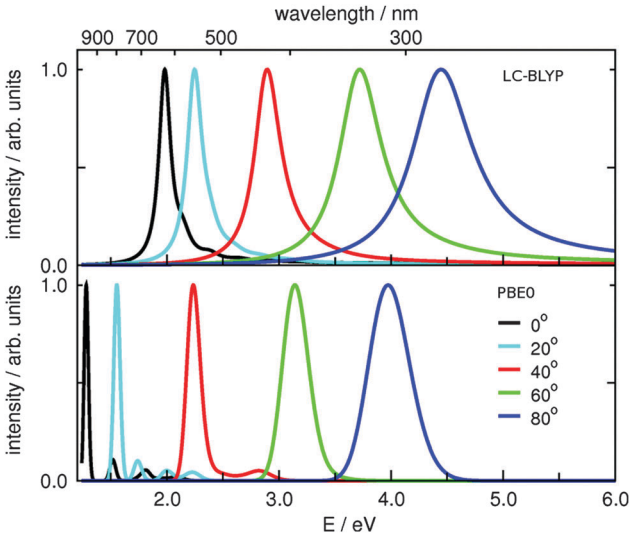

Fig. 9 Normalised theoretical absorption spectra of an idealized P3HT 32mer with fixed SCCS dihedral angles obtained with the LC-BLYP functional (top) and the PBE0 functional (bottom), respectively, together with the 6-31G* basis set. Hexyl groups were replaced by methyl groups.

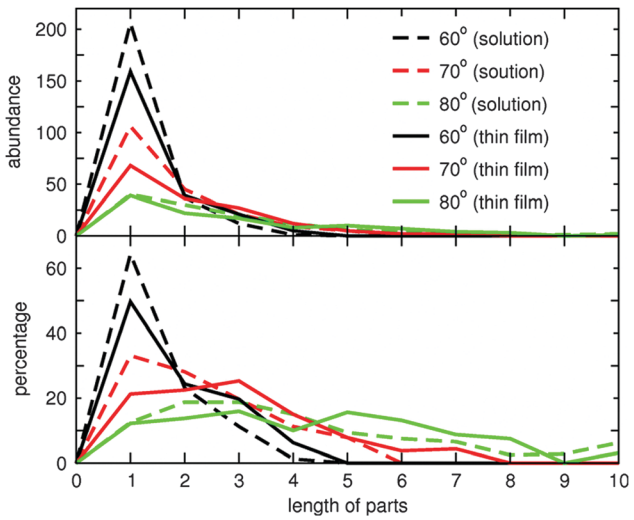

Fig. 10 Top: Distribution of conjugation lengths for the 10 selected molecules in solution (dashed lines) and the thin film (solid lines). The conjugation length l was defined as the length of a subchain in which the SCCS dihedral angles do not exceed a cut-off value of θ^{cut}. Results for $\theta^{cut} = 60^\circ$, $\theta^{cut} = 70^\circ$, and $\theta^{cut} = 80^\circ$ are shown. Bottom: Percentages of monomers belonging to subchains of different lengths for different cut-off angles θ^{cut}.

The distribution of the absolute SCCS dihedral angles, θ, relative to the ideal planar regioregular geometry, as a measure for out-of-plane distortion is plotted in Fig. 8 (red line). The histogram data shown (orange line) was obtained by collecting all SCCS dihedrals of all molecules in the unit cell at the final time frame of the simulation. A Gaussian fit to the histogram data using the function $a_1e^{-(\theta-b_1)^2/c_1} + a_2e^{-(\theta-b_2)^2/c_2}$ (red line) shows a maximum at $\theta = 62^\circ$.

Due to the out-of-plane distortion of the individual P3HT molecules, their π-electron system is less delocalized than in the ideal planar arrangement of the ordered crystal, causing a spectral blue-shift (Fig. 5). This effect can be illustrated by constructing a 32mer with fixed torsional angle θ between each pair of adjacent thiophene rings. Even for a moderate torsion angle of $\theta = 40^\circ$, the spectrum is blue-shifted by about 1 eV relative to $\theta = 0^\circ$ (see Fig. 9). It can further be seen that the spectral position is most sensitive in the region around $\theta = 60^\circ$. Therefore, this must coincide with the onset of severe perturbations to the π system. For torsion angles close to 90°, the individual thiophene rings are largely decoupled from each other as far as their π-electrons are concerned, resulting in spectral properties similar to those of the monomer.

In the following, we analyse the conjugation length in the P3HT molecules based on the torsional angle between adjacent thiophene rings. We divide each molecule into conjugated subchains inside which a SCCS dihedral cut-off angle, θ^{cut}, is not exceeded. For the 10 selected molecules, the top panel of Fig. 10 shows histograms of conjugation lengths l (in units of thiophene rings) obtained according to this definition for different values of θ^{cut}. A cut-off angle of 60° produces a relatively narrow distribution, where about half of the 320 thiophene rings counted are not part of a conjugated subchain, *i.e.* $l = 1$, 24% are part of a subchain of length $l = 2$, 20% are part of a subchain of length $l = 3$, and 6% are part of a subchain of length $l = 4$, while longer chains ($l > 4$) do not exist (Fig. 10, bottom panel). If the cut-off criterion for conjugation is increased to $\theta^{cut} = 70^\circ$, the distribution becomes significantly wider, with only 21% of thiophene rings not being part of a subchain ($l = 1$), 23% in $l = 2$ subchains, 25% in $l = 3$ subchains, 15% in $l = 4$ subchains, 8% in $l = 5$ subchains, and 4% in $l = 6$ and $l = 7$ subchains, respectively. For $\theta^{cut} = 80^\circ$, the distribution is broadened further, with 10% of thiophene rings now being in conjugated subchains of length longer than $l = 7$ at the expense of shorter chain with $2 \leq l \leq 4$.

The distribution of dihedral angles in the entire system (Fig. 8) shows that values between 60 and 70° occur with very

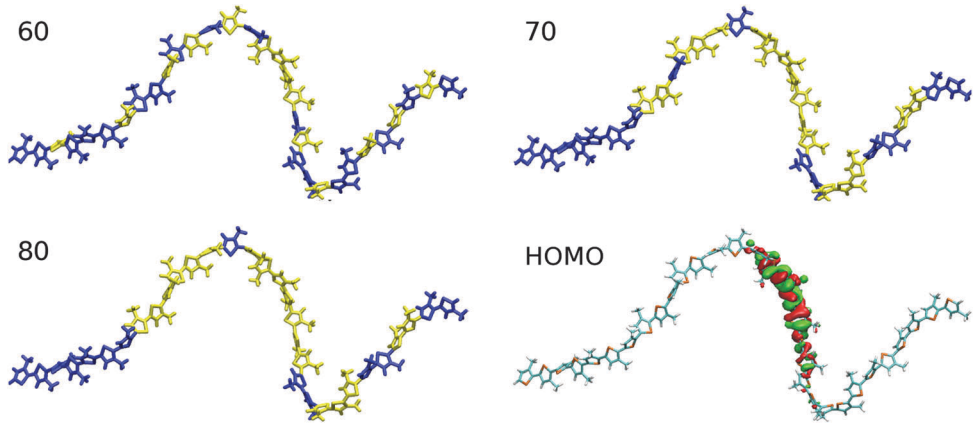

Fig. 11 Illustration of conjugated subchains for a selected molecule in the thin film. The conjugation length l was defined as the length of a subchain in which the SCCS dihedral angles do not exceed a cut-off value of θ^{cut}. The subchains obtained for θ^{cut} = 60°, θ^{cut} = 70°, and θ^{cut} = 80° are shown in different colors. In the bottom right corner, the HOMO orbital is visualized.

high abundance as this interval includes the maximum at 62°. Values of 80° are seen to be considerably less abundant.

The question is now which torsional angle cut-off produces conjugated subchains that match the shape of the molecular orbitals responsible for the spectral properties. In Fig. 11, we present a visual analysis for a selected molecule, which helps to narrow down the most suitable dihedral cut-off angle θ^{cut}. Since the main absorption peak is chiefly caused by a HOMO–LUMO transition, it is important to inspect the extent of delocalization in the HOMO. As Fig. 11 illustrates, the HOMO is delocalized over 7 thiophene rings situated near the center of the molecule. This situation is clearly not reflected by the subchains obtained with θ^{cut} = 60° (Fig. 11 top left). In this case, the 7-membered subchain on which the HOMO resides is subdivided into three fragments of length l = 1 and one fragment with l = 4. Cut-off criteria of θ^{cut} = 70° or θ^{cut} = 80° are both seen to produce a subchain of the right length to accommodate the HOMO (Fig. 11 top right and bottom left). At θ^{cut} = 84°, the 7mer in question merges with the dimer to its right to form a 9mer. Hence it appears reasonable to assume that the electronic properties of P3HT molecules are governed by subchains defined by cut-off torsional angles roughly in the region between 70 and 80°. The conjugation lengths obtained in this way are also consistent with the measured absorption peak around 2.4 eV (Fig. 5). Solving eqn (1) for the chain length at this energy yields n = 6.

So far we have exclusively linked the spectral properties to the torsional degrees of freedom. Further geometric analysis reveals that in the amorphous solid the molecules are also considerably bent. This can be seen from the distribution of end-to-end distances in Fig. 12 which is extremely broad and exhibits a maximum at 57 Å. For comparison, in an ideal planar geometry, the end-to-end distance is 121 Å. If the bending distortion were the dominant factor determining the position of the absorption spectrum, the thin film spectrum would have a larger shift relative to the ordered crystal than the solution phase, which only shows mild bending.

The above discussion emphasizes the need for an accurate force field representation of the torsional potential in order to accurately reproduce the absorption spectrum of P3HT. An illustration of the error introduced into the spectrum by an insufficient force field can be found in ref. 24.

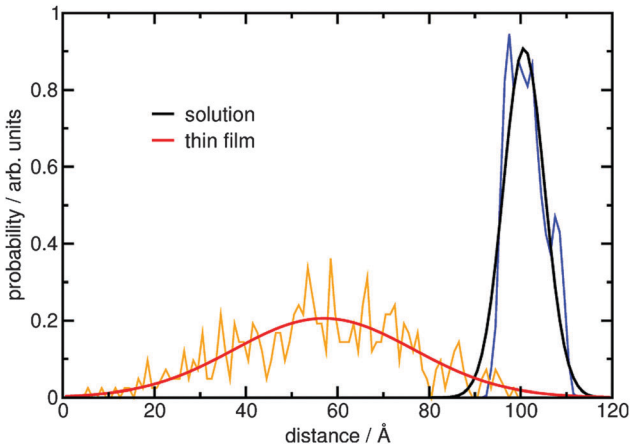

Fig. 12 Distributions of end-to-end distances (measured as the distance between the terminal C atoms). The histogram data for the thin film and the solution (orange and blue lines, respectively) is shown together with Gaussian fits of the form $ae^{-(x-b)^2/c}$ (red and black lines, respectively).

With the fragmentation of the π-system in the amorphous phase, long-range corrections in the TDDFT calculations are no longer required for all molecules. On the contrary, the use of range-separated functionals can introduce considerable errors in these cases. In Fig. 9 we compare the absorption spectra obtained with LC-BLYP and PBE0 for a 32mer with various torsion angles. It can be seen that for the perfectly planar geometry (θ = 0°), the PBE0 functional, which does not have the correct long-range behaviour, produces a significant red-shift compared to LC-BLYP from which we know that it reproduces experiment fairly well (see Fig. 5a). However, for large torsion angles, the situation is reversed. The long-range corrected LC-BLYP functional considerably overestimates excitation energies. To illustrate this we have performed TDDFT calculation on a thiophene monomer. Here, PBE0/6-31G* yields a 0–0 excitation energy of 5.4 eV, in fair agreement with the experimental value

of 5.2 eV,[57,58] while LC-BLYP/6-31G* gives 5.8 eV. Hence we chose to employ the PBE0 hybrid functional in the amorphous case in view of the reduced conjugation length.

3. Solution phase. The UV/Vis spectrum of P3HT in chloroform has been calculated by averaging over an ensemble of 10 configurations extracted from an MD simulation of a single 32mer in chloroform (see Section II for details). Fig. 5c shows that our theoretical and experimental absorption spectra are in fairly good agreement with each other. We mention in passing that TDDFT calculations for the same molecular structures without including the solvent *via* the PCM method yield virtually identical spectra (see ESI,† Fig. S4). Compared to the thin film, the maxima of both spectra are blue-shifted by about 0.35 eV to around 2.8 eV. This again correlates with the degree of inter-ring torsion within the polymers as our analysis suggests. The distribution of SCCS dihedral angles (Fig. 8) has a maximum at $\theta = 69^\circ$. The typical torsion angle is thus larger in the solution than in the amorphous solid. Consequently, the typical conjugation length is shorter in solution compared to the thin film. This is illustrated by the comparison of distributions of subchain lengths in Fig. 10. For a cut-off criterion of $\theta^{cut} = 60^\circ$, the vast majority (64%) are present as monomers. This is certainly at odds with the observed spectral position, as the monomer spectrum is expected at 6.2 eV according to eqn (1). If $\theta^{cut} = 70^\circ$ is used, the percentage of monomers reduces to 33%; the majority of thiophene rings are now in longer chains (28% dimers, 20% trimers, 11% tetramers, 8% pentamers). For $\theta^{cut} = 80^\circ$, the distribution of parts is considerably broadened with contributions up to $n = 10$ (Fig. 10). The highest percentages of rings are in dimers or trimers (19% each), 15% are in tetramers. The percentage curve (Fig. 10, bottom) tails off rather slowly with 6% of rings being in subchains of length $l = 10$. According to eqn (1), the spectral position of the solution phase near 2.8 eV corresponds to a chain length of $n = 4$. If one takes that to be the effective conjugation length in the longer chains, this would be consistent with the distribution of parts obtained for torsional cut-off angles near 80°. This is in line with the assessment for the thin film in Section IVB2, in particular the comparison to the molecular orbitals.

It is interesting to note that despite the fact that inter-ring torsion is more pronounced in solution, the molecules are much more stretched than in the thin film. The distribution of end-to-end distances shown in Fig. 12 peaks at 100 Å, close to the ideal planar geometry at 121 Å. This provides strong evidence that bending has a minor influence on the effective conjugation length, whereas torsion is by far more dominant.

Having established that the effective conjugation length in the solution phase is even shorter than in the amorphous thin film, it is clear that long-range corrections in the DFT calculations are not typically required (see also the discussion in the previous section (Section IVB2)), which is why the PBE0 functional was used here as well. Nevertheless, there is a minority of molecules (or configurations) that would be better described using a range-separated functional. The type of torsion-based conjugation length analysis presented here could be useful in deciding which method to choose for each individual configuration in future theoretical studies.

V. Conclusions

Optical absorption spectra of P3HT in three different phases–ordered crystalline, amorphous solid, and chloroform solution–have been computed using a multiscale approach linking coarse grained molecular dynamics, atomistic molecular dynamics and time-dependent density functional theory calculations. UV/Vis spectroscopic measurements have been performed of P3HT in solutions of chloroform ('good' solvent) and ethylacetate ('bad' solvent) in different mixing ratios. Considerable spectral changes, including a red-shift and a more structured shape, have been observed when changing from pure chloroform (100% good solvent) solutions to 50 : 50 mixtures. The latter exhibit all the features typically associated with amorphous thin films.

The theoretical spectra agree well with experimental data from our own measurements and from the literature, and reproduce the expected pronounced blue-shift from the crystal to the solution. This phenomenon could be correlated with the molecular conformation of the individual oligomers, in particular with the degree of torsion between adjacent thiophene rings. The effect of bending and the environment, *i.e.* molecular packing, was found to be minor. Since the spectral properties depend rather sensitively on molecular conformation, the force fields employed to generate the structures in the molecular dynamics simulations need to be very accurate in this respect. Hence we have reparametrized the force field using knowledge from density functional theory calculations.

In terms of the theoretical description of UV/Vis spectra, the single molecule approximation renders the calculation of optical absorption spectra in these complex condensed systems feasible. The choice of exchange–correlation functional used in the TDDFT calculations is crucial and depends on the extent of delocalization of the π-electrons, which in turn is determined by the molecular conformation and has to be assessed prior to each single molecule calculation. A partitioning scheme based on torsional angles is proposed to subdivide each molecule into conjugated subchains. This could be used in future DFT studies to make a sophisticated choice of functional for each individual configuration.

Acknowledgements

This project was partially funded by DFG within TRR 61. We are grateful for computer time at the high performance facilities of the University of Münster. We would like to thank Günter Reiter, Carlos Silva, and Frank Spano for providing us with their experimental data.

References

1 *Handbook of thiophene-based materials: applications in organic electronics and photonics*, ed. I. F. Perepichka and D. F. Perepichka, Wiley, Chichester, 2009, vol. 1.
2 J.-L. Brédas, J. E. Norton, J. Cornil and V. Coropceanu, *Acc. Chem. Res.*, 2009, **42**, 1691.

3 A. Mishra and P. Bäuerle, *Angew. Chem., Int. Ed.*, 2012, **51**, 2020.
4 M. Scharber and N. Sariciftci, *Prog. Polym. Sci.*, 2013, **38**, 1929.
5 U. Vongsaysy, D. Bassani, L. Servant, B. Pavageau, G. Wantz and H. Aziz, *J. Photonics Energy*, 2014, **4**, 040998.
6 S. D. Dimitrov and J. R. Durrant, *Chem. Mater.*, 2014, **26**, 616.
7 C. Poelking, K. Daoulas, A. Troisi and D. Andrienko, *Adv. Polym. Sci.*, 2014, **265**, 139.
8 N. Treat and M. Chabinyc, *Annu. Rev. Phys. Chem.*, 2014, **65**, 59.
9 E. G. McRae and M. Kasha, *J. Chem. Phys.*, 1958, **28**, 721.
10 R. M. Hochstrasser and M. Kasha, *Photochem. Photobiol.*, 1964, **3**, 317.
11 R. M. Hochstrasser, *Photochem. Photobiol.*, 1964, **3**, 299.
12 J. Gierschner, Y.-S. Huang, B. Van Averbeke, J. Cornil, R. H. Friend and D. Beljonne, *J. Chem. Phys.*, 2009, **130**, 044105.1.
13 P. B. Walczak, A. Eisfeld and J. S. Briggs, *J. Chem. Phys.*, 2008, **128**, 044505.1.
14 F. C. Spano, *J. Chem. Phys.*, 2005, **122**, 234701.
15 F. C. Spano, *J. Chem. Phys.*, 2007, **126**, 159901.
16 J. Clark, C. Silva, R. H. Friend and F. C. Spano, *Phys. Rev. Lett.*, 2007, **98**, 206406.
17 J. Clark, J. F. Chang, F. C. Spano, R. H. Friend and C. Silva, *Appl. Phys. Lett.*, 2009, **94**, 163306.
18 F. C. Spano and C. Silva, *Annu. Rev. Phys. Chem.*, 2014, **65**, 477.
19 K. Rahimi, I. Botiz, N. Stingelin, N. Kayunkid, M. Sommer, F. P. V. Koch, H. Nguyen, O. Coulembier, P. Dubois and M. Brinkmann, *et al.*, *Angew. Chem., Int. Ed.*, 2012, **51**, 11131.
20 K. Rahimi, I. Botiz, J. O. Agumba, S. Motamen, N. Stingelin and G. Reiter, *RSC Adv.*, 2014, **4**, 11121.
21 C. Scharsich, R. H. Lohwasser, M. Sommer, U. Asawapirom, U. Scherf, M. Thelakkat, D. Neher and A. Köhler, *J. Polym. Sci., Part B: Polym. Phys.*, 2012, **50**, 442.
22 F. Paquin, H. Yamagata, N. J. Hestand, M. Sakowicz, N. Bérubé, M. Côté, L. X. Reynolds, S. A. Haque, N. Stingelin and F. C. Spano, *et al.*, *Phys. Rev. B: Condens. Matter Mater. Phys.*, 2013, **88**, 155202.
23 H. Sirringhaus, P. J. Brown, R. H. Friend, M. M. Nielsen, K. Bechgaard, B. M. W. Langeveld-Voss, A. J. H. Spiering, R. A. J. Janssen, E. W. Meijer and P. Herwig, *et al.*, *Nature*, 1999, **401**, 685.
24 M. Böckmann and N. L. Doltsinis, *Frontiers in Materials*, 2015, **2**, 25.1.
25 N. L. Doltsinis, in *Computational Nanoscience: Do it Yourself!*, ed. J. Grotendorst, S. Blügel and D. Marx, NIC, FZ, Jülich, 2006, webarchiv.fz-juelich.de/nic-series/volume31/doltsinis3.pdf.
26 N. L. Doltsinis, in *Many-Electron Approaches in Physics, Chemistry and Mathematics*, ed. V. Bach and L. D. Site, Springer, Berlin, 2014, Mathematical Physics Studies.
27 M. J. Frisch, G. W. Trucks, H. B. Schlegel, G. E. Scuseria, M. A. Robb, J. R. Cheeseman, G. Scalmani, V. Barone, B. Mennucci and G. A. Petersson, *et al.*, *Gaussian 09, Revision D.01*, Gaussian, Inc., Wallingford, CT, 2009.
28 H. Iikura, T. Tsuneda and K. Hirao, *J. Chem. Phys.*, 2001, **115**, 3540.
29 A. D. Becke, *Phys. Rev. A: At., Mol., Opt. Phys.*, 1988, **38**, 3098.
30 C. Lee, W. Yang and R. C. Parr, *Phys. Rev. B: Condens. Matter Mater. Phys.*, 1988, **37**, 785.
31 C. Adamo and V. Barone, *J. Chem. Phys.*, 1999, **110**, 6158.
32 G. Scalmani and M. J. Frisch, *J. Chem. Phys.*, 2010, **132**, 114110.
33 M. Knipper, J. Parisi, K. Coakley, C. Waldauf, C. J. Brabec and V. Dyakonov, *Z. Naturforsch.*, 2007, **62a**, 490.
34 W. H. Lee, S. Y. Chuang, H. L. Chen, W. F. Su and C. Lin, *Thin Solid Films*, 2010, **518**, 7450–7454.
35 D. Van der Spoel, E. Lindahl, B. Hess, G. Groenhof, A. E. Mark and H. J. C. Berendsen, *J. Comput. Chem.*, 2005, **26**, 1701.
36 *Gromacs*, 2015, http://www.gromacs.org/.
37 C. M. Breneman and K. B. Wiberg, *J. Comput. Chem.*, 1990, **11**, 361.
38 A. D. Becke, *J. Chem. Phys.*, 1993, **98**, 5648.
39 R. S. Bhatta, Y. Y. Yimer, D. S. Perry and M. Tsige, *J. Phys. Chem. B*, 2013, **117**, 10035.
40 M. Moreno, M. Casalegno, G. Raos, S. V. Meille and R. Po, *J. Phys. Chem. B*, 2010, **114**, 1591.
41 R. S. Bhatta, Y. Y. Yimer, M. Tsige and D. S. Perry, *Comput. Theor. Chem.*, 2012, **995**, 36.
42 O. A. Gus'kova, P. G. Khalatur and A. R. Khokhlov, *Macromol. Theory Simul.*, 2009, **18**, 219.
43 G. Macchi, B. M. Medina, M. Zambianchi, R. Tubino, J. Cornil, G. Barbarella, J. Gierschner and F. Meinardia, *Phys. Chem. Chem. Phys.*, 2009, **11**, 984.
44 S. Pronk, S. Páll, R. Schulz, P. Larsson, P. Bjelkmar, R. Apostolov, M. R. Shirts, J. C. Smith, P. M. Kasson and D. van der Spoel, *et al.*, *Bioinformatics*, 2013, **29**, 845.
45 G. Bussi, D. Donadio and M. Parrinello, *J. Chem. Phys.*, 2007, **126**, 014101.
46 H. J. C. Berendsen, J. P. M. Postma, W. F. van Gunsteren, A. Di Nola and J. R. Haak, *J. Chem. Phys.*, 1984, **81**, 3684.
47 T. A. Wassenaar, K. Pluhackova, R. A. Böckmann, S. J. Marrink and D. P. Tieleman, *J. Chem. Theory Comput.*, 2014, **10**, 676.
48 S. J. Marrink and D. P. Tieleman, *Chem. Soc. Rev.*, 2013, **42**, 6801.
49 D. Janeliunas, PhD thesis, TU Delft, 2014, http://repository.tudelft.nl/view/ir/uuid.
50 D. Dudenko, A. Kiersnowski, J. Shu, W. Pisula, D. Sebastiani, H. W. Spiess and M. R. Hansen, *Angew. Chem., Int. Ed.*, 2012, **51**, 11068.
51 Z. Hu and A. J. Gesquiere, *Chem. Phys. Lett.*, 2009, **476**, 51.
52 W. Kuhn, *Helv. Chim. Acta*, 1948, **31**, 1780.
53 E. S. Manas and F. C. Spano, *J. Chem. Phys.*, 1998, **109**, 8087.
54 Y. Kim, S. Cook, S. M. Tuladhar, S. A. Choulis, J. Nelson, J. R. Durrant, D. D. C. Bradley, M. Giles, I. McCulloch and C.-S. Ha, *et al.*, *Nat. Mater.*, 2006, **5**, 197.
55 E. T. Niles, J. D. Roehling, H. Yamagata, A. J. Wise, F. C. Spano, A. J. Moulé and J. K. Grey, *J. Phys. Chem. Lett.*, 2012, **3**, 259.
56 P. J. Brown, D. S. Thomas, A. Köhler, J. S. Wilson, J.-S. Kim, C. M. Ramsdale, H. Sirringhaus and R. H. Friend, *Phys. Rev. B: Condens. Matter Mater. Phys.*, 2003, **67**, 064203.1.
57 J. Gierschner, J. Cornil and H.-J. Egelhaaf, *Adv. Mater.*, 2007, **19**, 173.
58 J. Gierschner, H.-G. Mack, H.-J. Egelhaaf and S. Schweizer, *Synth. Met.*, 2003, **138**, 311.